Chemistry–A European Journal
Full Paper
doi.org/10.1002/chem.202100787

Chemistry Europe
European Chemical Societies Publishing

Solvent-Dependent Stabilization of a Charge Transfer State is the Key to Ultrafast Triplet State Formation in an Epigenetic DNA Nucleoside

Xueli Wang[+],[a] Lara Martínez-Fernández[+],[b] Yuyuan Zhang[+],[c] Kun Zhang,[a] Roberto Improta,*[d] Bern Kohler,*[c] Jianhua Xu,[a, e] and Jinquan Chen*[a, e]

Abstract: 2′-Deoxy-5-formylcytidine (5fdCyd), a naturally occurring nucleoside found in mammalian DNA and mitochondrial RNA, exhibits important epigenetic functionality in biological processes. Because it efficiently generates triplet excited states, it is an endogenous photosensitizer capable of damaging DNA, but the intersystem crossing (ISC) mechanism responsible for ultrafast triplet state generation is poorly understood. In this study, time-resolved mid-IR spectroscopy and quantum mechanical calculations reveal the distinct ultrafast ISC mechanisms of 5fdCyd in water versus acetonitrile. Our experiment indicates that in water, ISC to triplet states occurs within 1 ps after 285 nm excitation. PCM-TD-DFT computations suggest that this ultrafast ISC is mediated by a singlet state with significant cytosine-to-formyl charge-transfer (CT) character. In contrast, ISC in acetonitrile proceeds via a dark $^1n\pi^*$ state with a lifetime of ~3 ps. CT-induced ISC is not favored in acetonitrile because reaching the minimum of the gateway CT state is hampered by intramolecular hydrogen bonding, which enforces planarity between the aldehyde group and the aromatic group. Our study provides a comprehensive picture of the non-radiative decay of 5fdCyd in solution and new insights into the factors governing ISC in biomolecules. We propose that the intramolecular CT state observed here is a key to the excited-state dynamics of epigenetic nucleosides with modified exocyclic functional groups, paving the way to study their effects in DNA strands.

Introduction

2′-Deoxy-5-formylcytidine (5fdCyd, Figure 1a), a well-known oxidation product of 5-methylcytidine has been identified as a naturally occurring nucleoside.[1] Recent studies show that 5fdCyd is generated by epigenetic modifications that can alter the DNA duplex structure, cell differentiation, and protein identification.[2] The formyl group introduces new chemical properties, which are absent in other cytosine derivatives, such as the formation of a Schiff base with histones[2c] and the high reactivity toward nucleophilic primary amines.[3] Moreover, 5fdCyd may mediate DNA-protein cross-link when it is in genomic DNA strands.[2d]

For the canonical DNA nucleosides, electronic energy is dissipated as heat on a time scale of several ps, following ultrafast internal conversion to the ground state.[4] However, chemical modifications at the C5 position of pyrimidines can significantly alter the excited state dynamics.[5] Prior transient absorption experiments on 5fdCyd revealed that the bright $^1\pi\pi^*$ state decays to a dark $^1n\pi^*$ state (located on the formyl group) on an ultrafast time scale in acetonitrile (ACN). The latter is a gateway state to a triplet state formed with an approximately 70% quantum yield.[6–7] Effective triplet-triplet

[a] X. Wang,[+] K. Zhang, Prof. J. Xu, Prof. J. Chen
State Key Laboratory of Precision Spectroscopy
East China Normal University
Shanghai 200241 (P. R. China)
E-mail: jqchen@lps.ecnu.edu.cn

[b] Prof. L. Martínez-Fernández[+]
Departamento de Química
Facultad de Ciencias and Institute for Advanced Research in Chemistry (IADCHEM)
Universidad Autónoma de Madrid
Campus de Excelencia UAM-CSIC
Cantoblanco, 28049 Madrid (Spain)

[c] Y. Zhang,[+] Prof. B. Kohler
Department of Chemistry and Biochemistry
The Ohio State University
100 West 18th Avenue, Columbus
Ohio 43210 (USA)
E-mail: kohler@chemistry.ohio-state.edu

[d] Prof. R. Improta
Istituto di Biostrutture e Bioimmagini CNR
Via Mezzocannone 16
80134 Napoli (Italy)
E-mail: robimp@unina.it

[e] Prof. J. Xu, Prof. J. Chen
Collaborative Innovation Center of Extreme Optics
Shanxi University, Taiyuan, Shanxi 030006 (P. R. China)

[+] These authors contributed equally to this work.

Supporting information for this article is available on the WWW under https://doi.org/10.1002/chem.202100787

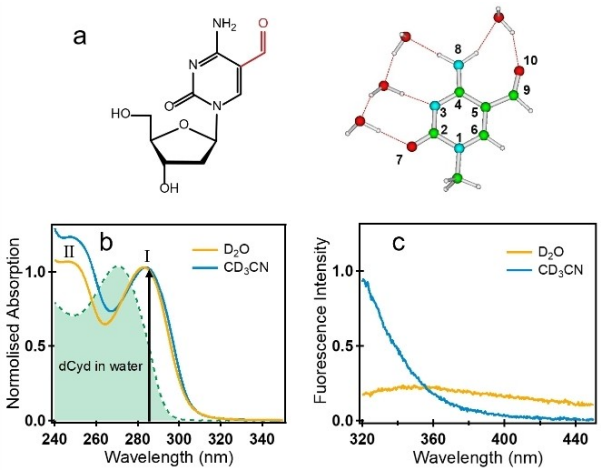

Figure 1. (a) Chemical Structures and computational model of 5fdCyd·$4H_2O$. (b) UV/Vis and (c) fluorescence spectra for 5fdCyd in D_2O/ACN.

energy transfer[8] has also been documented for 5fdCyd. Therefore, 5fdCyd has the potential to be an internal triplet photosensitizer which can initiate DNA photolesions. Although it has been reported that ISC in DNA nucleosides usually takes place from the singlet nπ* state to the lowest triplet ππ* state,[9] it was recently argued that ultrafast ISC can also occur from the initially populated bright ^{1}ππ* state to a higher energy triplet nπ* state,[10] and this mechanism may also exist in 5fdCyd. Yet, a full understanding of the ISC mechanism of 5fdCyd in solution is still missing.

In order to understand the mechanism responsible for the high triplet state quantum yield observed in 5fdCyd, excited state dynamics of 5fdCyd were investigated in aqueous phosphate buffered solution (PBS) and in ACN using time-resolved mid-infrared spectroscopy (TRIR) and quantum mechanical (QM) calculations. We show that several excited decay pathways coexist and that their interplay depends on the solvent. In PBS buffer, the excited-state population on the optically bright ^{1}ππ* state bifurcates to a charge-transfer (CT) state and a dark ^{1}nπ* state on an ultrafast time scale. ISC occurs from the CT state to a higher-energy triplet nπ* state. This pathway is not operative in ACN. Instead, the triplet state formation follows the 'traditional' mechanism where the singlet nπ* decays to the triplet ππ* state. Our results provide a comprehensive picture of the non-radiative excited state deactivation mechanism of 5fdCyd in solutions and show that an intramolecular CT state can regulate the excited state dynamics of DNA. It also suggests that 5fdCyd may be a versatile intermediate in DNA photo-dimerization reactions.[11]

Results

Steady-state absorption and emission spectra

Steady-state absorption spectra of 5fdCyd in D_2O buffered solution and ACN are shown in Figure 1b. In both solvents, the labile protons are replaced by deuterons (see details in the Experimental Section). In D_2O, two absorption peaks with similar intensity appear at 283 nm (hereafter band I) and 248 nm (band II). In ACN, band II is only slightly more intense than band I. Compared with absorption spectra of dCyd in the same solvents, the formyl substituent induces a red shift of ~0.2 eV for band I both in D_2O and ACN, whereas the shift is ~0.4 eV for band II.[5e,6] The fluorescence spectra of 5fCyd in water and in ACN following 285 nm excitation are shown in Figure 1c. Despite 5fdCyd has similar absorbance at 285 nm in both solvents, the shape and intensities of the corresponding fluorescence spectra are dramatically different. The emission spectrum of 5fdCyd in ACN exhibits a band centered below 320 nm and a tail that extends beyond 450 nm, and resembles that of dCyd.[5c,e] The D_2O emission spectrum shows instead a broader and weaker band with a peak centered at 350 nm. The fluorescence quantum yield of 5fCyd in ACN is similarly low as Cyd in ACN (on the order of 10^{-4}), but the quantum yield in D_2O is significantly lower than in ACN (Figure S1a).

Time-resolved IR spectroscopic data

Figure 2 displays the TRIR spectra for 5fdCyd in D_2O and ACN with 285 nm excitation. The difference spectra consist of negative bleach signals, which occur due to the depletion of the ground state population, and positive signals, which originate from vibrational modes of the excited states. For 5fdCyd in D_2O (Figure 2a–b), four bleaches are observed at frequencies that are in excellent agreement with band positions in the FTIR spectra. Meanwhile, five positive bands are seen at 1460, 1540, 1550, 1600 and 1710 cm^{-1}. As the positive band

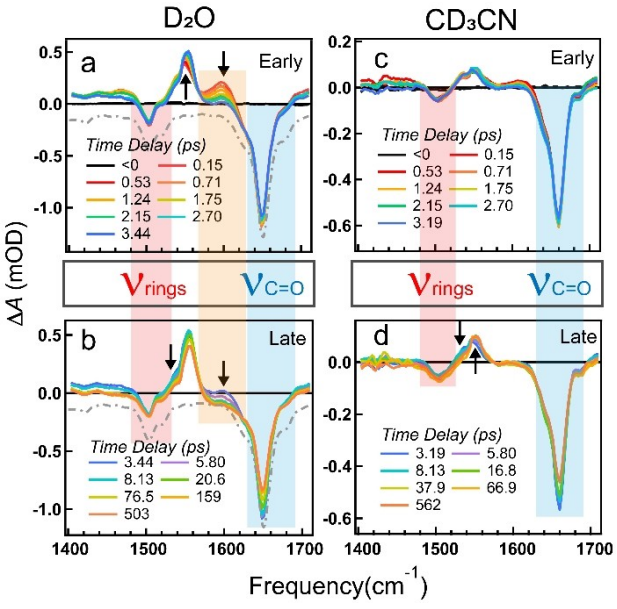

Figure 2. TRIR spectra at indicated delay times for deuterium exchanged 5fdCyd in D_2O buffer (a and b) and ACN (c and d) under 285 nm excitation. The inverted dot-dashed line shows the corresponding FTIR spectrum.

centered at 1600 cm^{-1} decays, the 1550 cm^{-1} band continues to increase in amplitude and blue shift to 1560 cm^{-1} in the first 3.5 ps (indicated by arrows in Figure 2a), resulting an isosbestic point at 1567 cm^{-1}. This suggests that a state-to-state transition occurs within the first ~4 ps after excitation. Over the next 10 ps, the 1600 cm^{-1} band continues to decay, while the 1550 cm^{-1} decays and slightly blue-shifts. After that, all bands decay slightly, yielding a long-lived spectrum that persists to 500 ps. In ACN, the TRIR spectra evolve very differently, especially at early times. As shown in Figure 2c, the initial TRIR signal shows two strong positive bands at 1540 and 1550 cm^{-1} along with a very weak band at 1610 cm^{-1}. Neither spectral shifting nor isosbestic points are observed in the first 3 ps. However, between 3 ps and 20 ps the 1540 cm^{-1} band decays while the 1550 cm^{-1} band increases with a discernable isosbestic point at 1545 cm^{-1} (Figure 2d).

Global analysis of the TRIR spectra in D_2O yielded three lifetimes (1.6 ± 0.1 ps, 2.9 ± 0.2 ps and 79 ± 4 ps) together with a constant component. The lifetimes in ACN obtained from global fitting are 3.9 ± 0.5 ps and 24.0 ± 3 ps plus a constant component. The evolution-associated difference decay spectra (EADS) corresponding to a sequential kinetic model are shown in Figure 3a-b. Decay traces at representative frequencies are shown in Figures 3d and S1b.

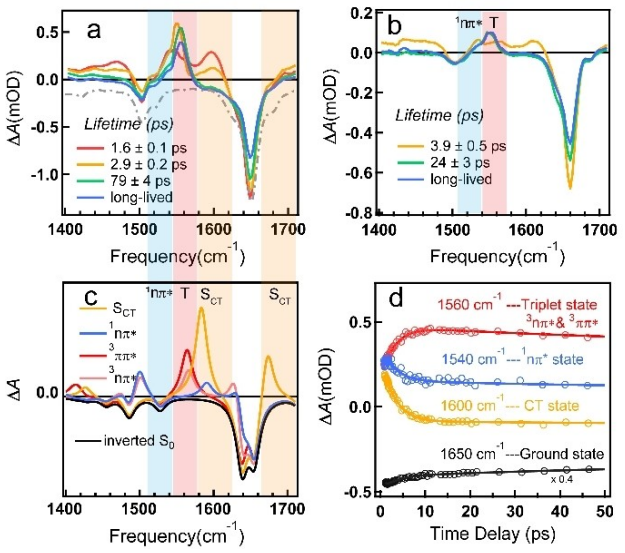

Figure 3. EADS of 5fdCyd in (a) D_2O and (b) CD_3CN. (c) Calculated DIR spectra of S_{CT}-min, S_1 $^1n\pi^*$min, T_2 $^3n\pi^*$-min and T_1 $^3\pi\pi^*$-min in D_2O. The inverted FTIR spectrum is shown for comparison. (d) Representative kinetics of 5fdCyd in D_2O.

Table 1. Vertical excitation energies computed in water for 5fCyt·$4H_2O$ and in ACN for 5fCyt at the PCM/TD-CAMB3LYP/6-311+G(2d,2p)//CAM-B3LYP/6-31G(d) level of theory. Oscillation strengths are shown in parentheses.

	S_1 ($^1n\pi^*_1$)	S_2 ($^1\pi\pi^*_1$)	S_3 ($^1\pi\pi^*_2$)	S_4 ($^1\pi\pi^*_3$)	S_5 ($^1n\pi^*_2$)
5fCyt·$4H_2O$ water	4.42 (0.00)	4.87 (0.29)	5.46 (0.17)	5.53 (0.11)	5.85 (0.06)
5fCyt in ACN	4.42 (0.00)	4.88 (0.31)	5.43 (0.11)	5.48 (0.17)	5.69 (0.00)

The excited states in the Franck-Condon (FC) region

The steady-state absorption spectra are assigned based on QM calculations (Table 1 and Table S1-2). The lowest energy excited state involves excitation from the lone pair of the formyl substituent to a π* orbital also mainly localized on the formyl moiety with some involvement of MOs of the Cyt ring. This state (labelled hereafter as $^1n\pi^*$) has an extremely low oscillator strength and thus is optically dark. The first bright state is S_2 ($^1\pi\pi^*_1$), which has a predominant HOMO→LUMO character (the associated natural transition orbitals (NTO) are depicted in Figure S2 in the Supporting Information). The $^1\pi\pi^*_1$ state is reminiscent of the lowest energy bright state in cytosine,[5e] which has a strong bonding/antibonding character with respect to the C5-C6 double bond (see Figure 1a for atom labelling), and a significant contribution from the formyl group. It is responsible for band I in the absorption spectrum. The second bright state (S_3, $^1\pi\pi^*_2$) has mainly HOMO-1→LUMO character. NTO analysis (Figure S2) reveals a very small contribution from the formyl group, indicating that this excited state has a small Cyt→formyl CT character. On the other hand, S_4 ($^1\pi\pi^*_3$), which involves electron promotion from the HOMO to the LUMO + 1, is antibonding with respect to the C2=O7, C4-N8 and C=O bonds. The close-lying $^1\pi\pi^*_2$ and $^1\pi\pi^*_3$ states (placed at 5.5 eV) are associated with band II, which is separated by ~0.6 eV with respect to band I (4.9 eV), in agreement with the experimental spectrum. The state order and energies are similar in ACN (Table 1).

Characterizing the excited state potential energy surfaces

We mapped the potential energy surface (PES) of the lowest energy excited states (both singlet and triplet), identified the singlet/singlet and singlet/triplet crossing regions and characterized their IR spectra both in water and ACN. A schematic description of the crossing regions is sketched in Figure 4. The optimized structures of the relevant minima are shown in Figure 5, and their main features are summarized in Tables S3–S4 and Figures S4–S7. For comparison, we mapped the PES using also the M052X functional in both solvents and in the gas phase at the MS-CASPT2 level (see Supporting Information). The latter is expected to provide a more accurate characterization of the intersystem crossing and internal conversion to the ground state mechanisms.

For water, 5fCyd is excited to the optically bright S_2 $^1\pi\pi^*_1$ state by a 285 nm photon. CAM-B3LYP excited state geometry optimization reaches a point where the excitation is mainly localized on the ring, and the molecule does not deviate significantly from planarity. This pseudo-minimum ($^1\pi\pi^*_1$-min-pla) is slightly less stable than the 'real' minimum ($^1\pi\pi^*_1$-min), which adopts a slightly bent conformation (Figure S4) and is very similar to the minimum of the lowest energy $^1\pi\pi^*$ state in

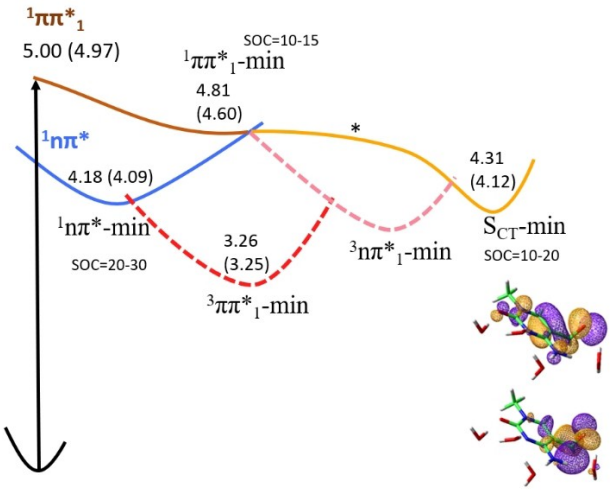

Figure 4. Schematic description of the main crossing and minima as computed by PCM/TD-CAM-B3LYP in water (adiabatic energies in parentheses) and in ACN. The * denotes the presence of an energy barrier on the path to S_{CT}-min, present only in ACN. Inset: Minima and NTO for the lowest energy singlet excited states of S_{CT}-min.

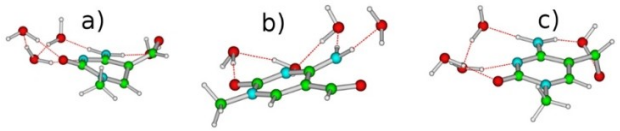

Figure 5. Schematic description of some minima computed in water at the PCM/TD-CAM-B3LYP/6-31G(d). (a) $^3\pi\pi^*_1$-min (b) $^1n\pi^*$-min (c) S_{CT}-min.

dCyd.[5e] The energy gap between $^1\pi\pi^*_1$-min and the $^1n\pi^*$ (S_1) state is only 0.10 eV at the same geometry. At $^1\pi\pi^*_1$-min, a triplet state (T_2) is also not far from S_2 (−0.8 eV), and the computed spin orbit coupling term (SOC) is not small (13 cm^{-1}) considering that, as discussed in the Supporting Information, TD-DFT appears to underestimate the SOC. T_2 has a predominant $^3n\pi^*$ character, though for a non-planar structure all of the lowest energy triplets (T_1, T_2 and T_3) are strongly mixed. Indeed, geometry optimization of T_2 leads to a T_1 $^3\pi\pi^*_1$-min, i.e. a minimum localized mainly on the ring, which is the triplet counterpart of the $^1\pi\pi^*_1$-min with a very distorted pyrimidine ring (see Figure 5).

Further geometry optimization from $^1\pi\pi^*_1$-min shows that another decay route exists for $^1\pi\pi^*_1$, leading to another minimum (now on the S_1 adiabatic surface), characterized by a 'perpendicular' arrangement of the formyl group with respect to the ring (Figure 5). In this region, S_1 can be described as an excitation from the Cyt HOMO, which interacts with the formyl lone pair, to the formyl π^* MO (Figure 5). Due to its non-negligible Cyt-Formyl CT character (0.2 a.u.), this minimum is labeled as S_{CT}-min. S_{CT}-min is flanked by two relatively close triplet states, i.e. T_1, (0.5 eV more stable) and T_2 (0.7 eV less stable). While the S_{CT}/T_1 SOC (2 cm^{-1}) is small, the SOC with T_2 is higher (13 cm^{-1}). These results, confirmed also by M052X, suggest that S_{CT} could act as a doorway state to the triplet manifold (see below). DFT geometry optimizations of T_2, when starting from S_{CT}-min leads to a minimum (labeled as $^3n\pi^*$-min) that can be described as an $n\pi^*$ excitation mainly localized on the formyl moiety and involving its lone pair ion ($^3n\pi^*$). The $^3n\pi^*$-min is slightly less stable than $^3\pi\pi^*_1$-min.

The S_2 $^1\pi\pi^*_1$ state can also decay to the S_1 $^1n\pi^*$ state. Geometry optimization of the $^1n\pi^*$ state leads to a minimum ($^1n\pi^*$-min), where the C=O bond length increases to 1.30 Å from 1.22 Å at the FC geometry, and the formyl moiety is strongly pyramidalized. The NTO of $^1n\pi^*$-min involves the transfer from the lone pair of the formyl O atom to the π^* formyl MO (Figure S5) with a small contribution from the ring. It is rather close to the T_1 (energy gap 0.5 eV) and T_2 states (energy gap 0.4 eV). The SOC with T_1 is rather high (15 cm^{-1}) and that with T_2 is even larger (22 cm^{-1}), suggesting that population transfer to T_2 is possible, with final transfer to the T_1 $^3\pi\pi^*_1$-min.

An extensive exploration of the PES in ACN provides a picture similar to that obtained in water, but with one crucial difference (Figure 4). In ACN the formyl group and the aromatic ring are locked in a nearly planar conformation to maintain the intramolecular hydrogen bond between the formyl and the amino groups. Consequently, access to the S_{CT}-min is more difficult because it requires out-of-plane motion by the formyl group, as mirrored by the presence of an energy barrier of ~0.10 eV in the path leading to S_{CT}-min. Moreover, the relative stability of this latter minimum with respect to $^1n\pi^*$-min is 0.1 eV lower than in water (0.13 vs 0.03 eV). In ACN, the most effective decay path for the $^1\pi\pi^*_1$ population involves transfer to $^1n\pi^*$-min or to T_2 and ultimately to T_1. As discussed in detail in the Supporting Information, the picture obtained in the gas phase at the MS-CASPT2 level (see Figure S7) is consistent with that just described, considering the role of environmental effects. In the gas phase, both CAM-B3LYP and M052X provide a description of the PES similar to that of MS-CASPT2 except for a general underestimation of the SOCs, further supporting the reliability of the picture obtained in solution.

Finally, we have characterized the crossing region with the ground electronic state and both $^1\pi\pi^*_1$ and $^1n\pi^*$ states. In solution we have verified (see Supporting Information for details) that both in water and in ACN a sizeable energy barrier (0.15 ~ 0.20 eV) separates $^1\pi\pi^*_1$-min from the lowest energy ethylenic-like crossing region, i.e. the region ruling the ultrafast excited state deactivation in cytosine and its derivatives.[5e,12] On this ground, we predict that decay to the lower lying singlet and triplet excited states is particularly effective and that the $^1n\pi^*$ state should be the singlet state most involved in non-radiative deactivation to S_0. The lowest energy crossing region between $^1n\pi^*$ and S_0 is characterized by a significant puckering of the ring and it is more than 0.5 eV less stable than $^1n\pi^*$-min both in water and in ACN. This conclusion is supported by MS-CASPT2 calculations in the gas phase, which we performed to locate the lowest energy $S_0/^1\pi\pi^*_1$ and $S_0/^1n\pi^*$ Conical Intersections (CI). They are significantly less stable than $^1\pi\pi^*_1$-min (by 0.90 eV) and $^1n\pi^*$-min (by 0.56 eV) (see also Supporting Information).

Computed IR spectra at the different minima

The harmonic IR spectra associated with the different minima were computed at the PCM/TD-CAM-B3LYP/6-31G(d) and PCM/TD-M052X/6-31G(d) (reported in the Supporting Information) level of theory in ACN and D_2O (see Experimental Methods Section for details). Difference IR (DIR) spectra were computed by subtracting the IR spectrum of S_0 calculated at the same level of theory. The results are shown in Figure 3c (D_2O/CAM-B3LYP) and Figures S8-S11 (ACN and M052X).

Starting our analysis with the case of D_2O, the DIR spectrum computed for S_{CT} (yellow trace, Figure 3c) shows a strong positive band centered at 1580 cm^{-1}, which is assigned to a collective ring stretching. A less intense positive peak at 1670 cm^{-1} due to stretching of the CO group on the pyrimidine ring is also observed. The aromatic ring is partially positively charged in S_{CT}-min and blue-shifting of the CO stretch frequency in positively charged nucleobases has been reported previously.[13] The calculated DIR spectrum for S_1 $^1n\pi^*$-min (blue trace) shows just two weak positive bands at 1590 cm^{-1} and 1500 cm^{-1}. Both modes are assigned to collective ring stretching, while the 1500 cm^{-1} mode has a contribution from amino group stretching. DIR spectra of the two lowest-energy triplet minima were calculated. The DIR of the lowest energy T_1 $^3\pi\pi^*_1$-min (red trace) exhibits a strong positive peak at 1560 cm^{-1}, which is assigned to ring stretching with a strong contribution from the amino group. For T_2 $^3n\pi^*$-min (pink trace), the calculation predicts a peak at 1560 cm^{-1} and another one at 1500 cm^{-1} due to ring stretching modes.

Discussion

Distinct ISC channels for 5fdCyd in water versus ACN

To understand ISC for 5fdCyd in water and ACN, the experimental and calculated results are compared in Figure 3 with the colored areas indicating matching absorption features. In water, the vibrational marker bands diagnostic of the S_{CT}-min (1585 and 1670 cm^{-1}) are visible in the initial TRIR spectra (Figure 3). These bands directly evolve into the marker band at 1550 cm^{-1}, which belongs to the triplet state. Kinetics shown in Figure 3d clearly demonstrate that the decay of S_{CT} (yellow trace) is correlated with the build-up of triplet states (red trace). Considering the larger SOC strength, we assign the ultrafast ISC to the transition from S_{CT}-min to the T_2 ($^3n\pi^*$) state. As mentioned above, a clear blue-shift of the triplet marker band (~1560 cm^{-1}) is seen when the second EADS evolves to the third one. Combined with calculations, this spectral evolution suggests that the T_1 ($^3\pi\pi^*$-min) state is also populated on a later timescale (second EADS evolves to the third). The combination of experiment and theory offers evidence of CT induced triplet state generation in 5fdCyd. This assignment is also supported by the PES calculations. As shown in Figure 4, a dark state (S_{CT}) with Cyt to formyl group charge transfer character is present in 5fCyt • $4H_2O$ that can only be accessed when the formyl group is significantly displaced from the pyrimidine ring (in the minimum it is perpendicular to the ring). The adiabatic energy minimum of S_{CT} is almost as low as that of the S_1 ($^1n\pi^*$) state, suggesting that it is possible to populate these two dark states after 5fdCyd is excited to the bright S_2 ($^1\pi\pi^*_1$) state. Considering the SOC and energy difference, the transition from S_{CT} to T_2 ($^3n\pi^*$) is the most probable channel for the observed ultrafast ISC when 5fdCyd is in D_2O.

For ACN, it is obvious that the marker bands for S_{CT}-min (1585 and 1670 cm^{-1}) are missing even in the first EADS. Comparison with the calculated spectrum of the $^1n\pi^*$ state suggests that this component is mainly due to the S_1 $^1n\pi^*$ state. The positive features in this EADS could be assigned to the $^1\pi\pi^*$-min and $^1\pi\pi^*$-min-pla according to the DIR spectra, but internal conversion from the S_2 ($^1\pi\pi^*$) state to the S_1 ($^1n\pi^*$) state is expected to be very fast. Moreover, this 3.9 ps lifetime also contains information of vibrational cooling of the hot $^1n\pi^*$ state. Because of the strong positive band centered at 1550 cm^{-1}, the second (24 ps) and the long-lived components are assigned to the triplet T_1 $^3\pi\pi^*$. The isosbestic point between the first and second EADS indicates that in ACN the $^1n\pi^*$ acts as gateway state for the population of the T_1 $^3\pi\pi^*$ triplet state in line with conclusions from the literature.[6–7] However, the ground state bleach kinetics suggests that the 24 ps component should also contain signal from a minor decay channel to the ground state (see below).

Our calculations also predict that both in water and ACN $^1\pi\pi^*_1$-min has a significant SOC (13 cm^{-1}) with a triplet state (T_2) that is somewhat lower in energy (−0.8 eV). This channel may also exist because the positive band for the triplet state at ~1550 cm^{-1} can be detected both in water and ACN at very early time delays. However, we cannot definitively confirm this at the present time because our limited time resolution prevents us from obtaining TRIR and DIR spectra of $^1\pi\pi^*_1$-min.

Our study also provides new insights on the nonradiative decay pathways not involving triplet states. In detail, we show that in both solvents decay components of a few dozens of ps are present. We propose that, besides ISC to triplets, an additional decay channel is available for the excited state population from the bottom of the dark $^1n\pi^*$ state according to the ground state bleaching kinetics (Figure 3d and S1). It is worth pointing out that similar lifetime was observed for the dark state in dCyd. However, in dCyd, this dark state, which has been proposed to also be active in DNA duplexes,[14] involves the lone Pair of the O7 atom in the pyrimidine ring and not the formyl substituent.[15]

Our prediction that an additional decay channel is available for the decay of the $^1\pi\pi^*$ minimum in water is consistent with the strong solvent-dependence of the fluorescence spectrum. In water, the larger conformational flexibility of the formyl group, which modulates the coupling of the bright emissive $^1\pi\pi^*$ with the dark S_{CT} state, enables emission from a wider region of the PES. This explains the weaker, broader, and red-shifted fluorescence spectrum observed in water. As discussed in the Supporting Information, the energy difference between the anti-conformer (where the formyl and amino groups are in anti-arrangement) and the most stable syn one (shown in Figure 1) is smaller in water than in ACN. This minor conformer,

whose population should be larger in water, is characterized by red-shifted emission with respect to the anti-conformer (see Supporting Information). Finally, a state with partial CT character is expected to be more sensitive to the solvent arrangement and, therefore characterized by enhanced solvent inhomogeneous broadening.[16]

Charge transfer-induced intersystem crossing

The photophysics and photochemistry of aromatic ketones and aldehydes such as benzophenone and benzaldehyde have been extensively studied for decades.[17] It is commonly accepted that ISC in these molecules is facilitated by a large spin-orbit matrix element together with a small energy barrier between the $^1n\pi^*$ and $^3\pi\pi^*$ states. For the simplest aromatic carbonyl molecules, such as benzaldehyde and acetophenone, the S_1 ($^1n\pi^*$) state is almost degenerate with the two lowest-lying triplet states, and this could lead to efficient ISC after photo-excitation.[17b] Moreover, high level calculations have predicted that for a wide variety of aromatic carbonyl compounds the $S_1/T_1/T_2$ crossing region is only 4–6 kcal mol^{-1} above the minimum of the S_1 state.[17d] This region can be easily accessed by breaking the conjugation between the carbonyl substituent and the ring. Thus, ISC in these molecules takes place easily and rapidly ($k_{ISC} \sim 10^{10}$ s^{-1}).[17d] We propose that ISC for 5fdCyd in ACN occurs similarly.

For 5fdCyd in water, the fluorescence spectrum, which is broader and red-shifted compared to in ACN, and the blue-shift of the C=O band in the TRIR data signal the involvement of a CT state. This conclusion is further confirmed by our QM calculations, showing that an energy minimum (S_{CT}-min) with Cyt to formyl CT character is reached when the formyl group and the cytosine ring are nearly orthogonal (Figure 4). Following 285 nm excitation, a significant part of the population on the $^1\pi\pi^*$ surface decays to this minimum (Figure 3), which is nearly isoenergetic with the lowest minimum in the singlet manifold ($^1n\pi^*$-min). There are three possible decay pathways for the excited state population in S_{CT}-min. The first two lead to the ground state by fluorescence or internal conversion, while the third is ISC to the triplet state. The ground state bleaching signal at 1650 cm^{-1} (Figure 3d) shows little decay in the first several picoseconds, suggesting that there is minimal decay to the ground state during the time interval when ISC from the S_{CT} state takes place. The triplet quantum yield of 5fdCyd in aqueous solution is therefore expected to be high, possibly even higher than the reported value of 70% in ACN.[6]

Triplet formation from a CT state, which has not been described previously in nucleobases to the best of our knowledge, may proceed via either of two mechanisms. In the spin-orbit CT ISC (SOCT-ISC) mechanism,[18] changes in orbital angular momentum must be compensated by changes in spin angular momentum due to the conservation of total angular momentum. The orthogonal structure of the C=O group and the cytosine ring can fulfill the requirement for a change in orbital angular momentum when charge recombination is involved.[19] Recently, there have been several reports of fast SOCT-ISC and high triplet quantum yields in molecular dyads with orthogonal donor and acceptor structures.[20] As discussed above, the orthogonal conformation between the C=O group and the cytosine ring is only reachable when 5fdCyd is in water. The SOC strength is found to be 10–20 cm^{-1} between the CT state and the triplet state. It is worth noting that the SOC is at least 1–2 order of magnitude larger than values reported for BODIPY dyads, consistent with the ultrafast ISC observed here.[20g] All these pieces of evidence make a strong case for SOCT-ISC as a possible explanation of ultrafast ISC in 5fdCyd.

Another possible mechanism for CT-induced ultrafast ISC in 5fdCyd is spin-vibronic coupling. It is shown that the energy of S_{CT}-min is ~0.5 eV lower than $^1\pi\pi^*$-min, which could enhance the coupling between this region of the PES and the low-lying triplet states. The almost perpendicular geometry between the formyl group of 5fdCyd and the pyrimidine ring in S_{CT}-min that facilitates a spin flip during charge recombination as described above is also expected to enhance coupling of this singlet state to a nearby triplet state. It has been reported that out-of-the-plane motions can promote the spin-vibronic coupling between the bright $^1\pi\pi^*$ state and triplet states (both $^3\pi\pi^*$ and $^3n\pi^*$), leading to ultrafast ISC in thio-bases.[21,22] Therefore, it is also plausible that the key to the ultrafast ISC in 5fdCyd is the matched energy level between S_{CT} minimum and T_2 ($^3n\pi^*$) together with the orthogonal structure of the carbonyl group which enhances vibronic coupling between these two states.

According to our analysis, the solvent has a dramatic influence on the photoexcited state behavior of 5fdCyd. As discussed in the previous section, its fluorescence properties are very different in D_2O and in the polar, yet non-hydrogen-bonding solvent ACN. Although triplet yields are high in both solvents, our results show that ISC happens even more rapidly in aqueous solution where it is mediated by a gateway CT state that is hardly observed in ACN.

Solute-solvent hydrogen bonds play a key role in these differences. As shown in Figure 4 and Figure 5, the minimum with CT character in water is stabilized by an orthogonal geometry. In ACN, this geometry is difficult to access because of the stable intramolecular hydrogen bond between the carbonyl and the $-NH_2$ group, which leads to the presence of an energy barrier in the path leading to S_{CT}-min. This strongly reduces its involvement in the decay of 5fdCyd in ACN, and ISC follows expectations for the gas phase. Solvent effects on fluorescence lifetimes of nucleobases are well known,[23] but this is the first example to our knowledge where solvent-dependent stabilization of a CT state facilitates ultrafast ISC. Understanding the reactivity of 5fdCyd in duplex DNA, where a large variety of intra- and intermolecular hydrogen bond interactions are present, is a worthy challenge for the future.

Conclusion

In the present study, we investigated the excited state dynamics of 5fdCyd in water and ACN by TRIR and QM calculations. The different rates of ISC measured in buffer versus ACN solution are attributed to different decay pathways. In buffer, a CT state

with an orthogonal geometry between the formyl group and the cytosine ring is formed initially, which can promote effective ISC $^3n\pi^*$ state with a <1 ps lifetime. This ISC channel do not work in ACN due to the limitation of intramolecular hydrogen bond, which leads to the presence of an energy barrier to access the S_{CT}-min. Our results set the stage for investigating excited states of 5fdCyd incorporated into DNA strands. It remains to be seen what effects the restricted access to water molecules and other intramolecular interactions (such as proton coupled electron transfer) in the different DNA double strands will have on excited state dynamics by this epigenetically significant cytosine derivative. Finally, we note that a full understanding of ISC mechanisms by small molecules in a DNA environment is a necessary step on the path to designing useful photosensitizers for biological applications.

Experimental Section

Experimental methods

Chemicals: 2′-Deoxy-5-formylcytidine ($\geq$97%) was purchased from Berry and Associates, Inc. Phosphate buffer solution (25 mM NaH_2PO_4 and 25 mM Na_2HPO_4) was prepared in D_2O (Sigma-Aldrich, 99.9% D). CD_3CN was purchased from Sigma-Aldrich (>99.9% atom D).

For the TRIR experiments in D_2O, 4.6 mg of 2′-deoxy-5-formylcytidine (5fCyd) was dissolved in 3 mL 50 mM phosphate buffer solution (PBS) prepared in D_2O. The concentration was 6 mM. For the TRIR experiments in CD_3CN, approximately 5.0 mg of 5fCyd was first dissolved in D_2O for deuterium exchange of the labile protons. The solution was subject to freeze-drying for 24 hrs. 3 mL CD_3CN was added to the resulting dry solid. Due to the limited solubility of 5fCyd in CD_3CN, the mixture was allowed to settle and the supernatant, which contained the saturated 5fCyd solution, was taken for experiments.

Steady-state absorption spectroscopy: Steady-state UV-visible absorption spectra were measured at room temperature using a JASCO J-815 CD spectrometer. The D_2O and CD_3CN solutions were held in fused silica cells with 100 μm and 1 mm optical path length, respectively.

Fourier-transformed IR (FTIR) spectra were measured using a JASCO FTIR 4200 spectrometer. The D_2O and CD_3CN solutions were held in CaF_2 cells with 100 μm and 500 μm optical path length, respectively.

The concentrations used in the steady-state absorption experiments were identical to those used in the time-resolved experiments (see below). All steady-state absorption spectra shown in the main text have been corrected for solvent background.

Fluorescence: The steady-state fluorescence spectra were recorded using a Horiba PTI-QM-8075-22-C spectrofluorometer. The fresh, concentrated solutions in D_2O and CD_3CN (described above) were diluted to give absorbance at 285 nm (A285) of 0.23 and 0.19, respectively, measured in a 1 cm fused silica cell. The samples were excited at 285 nm and the fluorescence signal was recorded from 300 nm to 450 nm. All slits in the excitation and detection monochromators were adjusted to give a 5 nm bandwidth. The intense Raman signals at 304 nm (CD_3CN) and 307 nm (D_2O) have been removed for clarity. All spectra have been corrected for instrument sensitivity and background signals from the solvent.

Time-resolved IR spectroscopy (TRIR): The TRIR spectrometer has been described in detail before.[24] Briefly, the 285 nm pump was generated by an optical parametric amplifier (OPerA Solo, Coherent Inc). The prerequisite 570 nm was generated by sum-frequency mixing of the idler and the fundamental 800 nm (3.5 W, 90 fs, 1 kHz; Libra-HE, Coherent Inc). The visible pulses were subsequently frequency-doubled in a BBO crystal. Every other pump pulse was blocked by an optical chopper operating at 500 Hz. The pump pulse was attenuated to 1.2 μJ/pulse using a fused silica neutral density filter, and focused to a spot size of 430 μm (fwhm) at the sample position using a fused silica lens.

The broadband mid-IR probe pulses centered at 6150 nm (1626 cm^{-1}) and 6800 nm (1470 cm^{-1}) were generated by difference frequency mixing of the signal and idler pulses from a second optical parametric amplifier (OPerA Solo + nDFG, Coherent Inc). The probe beam was split into two portions, signal and reference, for multichannel referencing to improve the signal-to-noise ratio. Both portions were focused onto the sample, but only the signal beam overlapped with the pump beam. Both portions were subsequently recollimated and refocused into a spectrograph (Triax, Horiba), dispersed by a 100 lines/mm grating blazed at 6000 nm, and projected onto a liquid N_2-cooled, dual-row, 64-element/row HgCdTe detector (Infrared Systems Development).

The relative polarization of the UV pump and the mid-IR probe pulses was set to magic angle (54.7°). The pump-probe delay was varied using a 60 cm optical delay stage, which gave a total of 4 ns delay. The sample was recirculated in a flow cell (Harricks). For the D_2O experiments, a 100 μm-thick Teflon spacer, which defined the optical path length of the sample, was placed between two CaF_2 windows. The optical path length was 500 μm for the CD_3CN experiments. The sample concentration for D_2O experiments was 6 mM. The concentration of the saturated 5fCyd solution in CD_3CN was estimated to be 0.7 mM, assuming that the extinction coefficient at 285 nm (ε285) is identical to that in D_2O.

To analyze the TRIR date, experimental spectra from 0.3 ps to 3.6 ns were subject to global analysis using the Glotaran software package.[25] The EADS obtained from target analysis by sequential model are displayed in Figure 3 A and B. The representative kinetics are shown in Figure 3B and Figure S1. The lifetime uncertainties reported in the main text are twice the standard deviation.

Computational methods: Our calculations were performed on the model depicted in Figure 1, where the sugar is mimicked by a methyl group and the formyl group is syn with respect to the amino group. Excited state potential energy surfaces were computed by Time Dependent Density Functional Theory (TD-DFT) using two different functionals: CAM-B3LYP[26] and M052X.[27] Unless specified in the main text, the CAM-B3LYP results are discussed. Optimizations were done by using the 6–31G(d) basis set, checking for the effect of the basis set by single point calculations with a larger basis set. Bulk, solvent effects, both in water and in ACN, are included using the polarizable continuum (PCM) model,[28] whereas the effect of hydrogen bond interactions were considered by explicitly including four D_2O molecules with the arrangement shown in Figure 1. This procedure has been profitably used to study the photoactivated behavior of nucleobases in solution,[29,23a] including Cyt derivatives.[5e,f][30] SOC terms were computed using the pysoc program.[31] See Supporting Information for further details about DFT and CASPT2 calculations.

The IR spectrum for the relevant ground and excited state minima were computed at the harmonic level. To account for the lack of modelling of anharmonic effects and to facilitate comparison with experiments, all frequencies were uniformly scaled by 0.955, using

a procedure commonly used in the literature,[13b,32] and the labile protons were substituted with deuterons.

Acknowledgements

This study was funded by National Nature Science Foundation of China (No. 21873030, 11674101 and 91850202 to J.C.), Shanghai Rising-Star Program (No. 19QA1402800 to J.C. and supported by the 111 Project (B12024). Work at Ohio State University was supported by the U.S. National Science Foundation (CHE-1800471) and by funding from The Ohio State University. L.M.F. thanks the PID2019-110091GB-I00 (MICINN) project for financial support and the Centro de Computación Científica UAM (CCC-UAM) for computing time.

Conflict of Interest

The authors declare no conflict of interest.

Keywords: DNA photophysics and photochemistry · charge transfer states · epigenetic nucleoside · intersystem crossing · triplet excited states

[1] S. Ito, L. Shen, Q. Dai, S. C. Wu, L. B. Collins, J. A. Swenberg, C. He, Y. Zhang, *Science* **2011**, *333*, 1300–1303.
[2] a) E. A. Raiber, P. Murat, D. Y. Chirgadze, D. Beraldi, B. F. Luisi, S. Balasubramanian, *Nat. Struct. Mol. Biol.* **2015**, *22*, 44–49; b) M. Bachman, S. Uribe-Lewis, X. Yang, H. E. Burgess, M. Iurlaro, W. Reik, A. Murrell, S. Balasubramanian, *Nat. Chem. Biol.* **2015**, *11*, 555–557; c) E.-A. Raiber, G. Portella, S. Martínez Cuesta, R. Hardisty, P. Murat, Z. Li, M. Iurlaro, W. Dean, J. Spindel, D. Beraldi, Z. Liu, M. A. Dawson, W. Reik, S. Balasubramanian, *Nat. Chem.* **2018**,*10*,1258–1266; d) F. Li, Y. Zhang, J. Bai, M. M. Greenberg, Z. Xi, C. Zhou, *J. Am. Chem. Soc.* **2017**, *139*, 10617–10620.
[3] a) B. Xia, D. Han, X. Lu, Z. Sun, A. Zhou, Q. Yin, H. Zeng, M. Liu, X. Jiang, W. Xie, *Nat. Methods* **2015**, *12*, 1047–1050; b) B. Samanta, J. Seikowski, C. Höbartner, *Angew. Chem. Int. Ed.* **2016**, *55*, 1912–1916; *Angew. Chem.* **2016**, *128*, 1946–1916.
[4] a) C. E. Crespo-Hernández, B. Cohen, P. M. Hare, B. Kohler, *Chem. Rev.* **2004**, *104*, 1977–2019; b) M. Barbatti, A. C. Borin, S. Ullrich, *Top. Curr. Chem.* **2014**, *355*, 1–32; c) R. Improta, F. Santoro, L. Blancafort, *Chem. Rev.* **2016**, *116*, 3540–3593.
[5] a) R. J. Malone, A. M. Miller, B. Kohler, *Photochem. Photobiol.* **2003**, *77*, 158–164; b) A. Nakayama, S. Yamazaki, T. Taketsugu, *J. Phys. Chem. A* **2014**, *118*, 9429–9437; c) C. Ma, C. C.-W. Cheng, C. T.-L. Chan, R. C.-T. Chan, W.-M. Kwok, *Phys. Chem. Chem. Phys.* **2015**, *17*, 19045–19057; d) B. Marchetti, T. N. V. Karsili, M. N. R. Ashfold, W. Domcke, *Phys. Chem. Chem. Phys.* **2016**, *18*, 20007–20027; e) L. Martinez-Fernandez, A. J. Pepino, J. Segarra-Martí, J. Jovaisaite, I. Vayá, A. Nenov, D. Markovitsi, T. Gustavsson, A. Banyasz, M. Garavelli, R. Improta, *J. Am. Chem. Soc.* **2017**, *139*, 7780–7791; f) L. Martinez-Fernandez, A. Banyasz, L. Esposito, D. Markovitsi, R. Improta, *Signal Transduction Targeted Therapy* **2017**, *2*, 17021; g) A. J. Pepino, J. Segarra-Martí, A. Nenov, I. Rivalta, R. Improta, M. Garavelli, *Phys. Chem. Chem. Phys.* **2018**, *20*, 6877–6890; h) Z. Zhou, X. Zhou, X. Wang, B. Jiang, Y. Li, J. Chen, J. Xu, *J. Phys. Chem. A* **2017**, *121*, 2780–2789; i) X. Wang, Z. Zhou, Y. Tang, J. Chen, D. Zhong, J. Xu, *J. Phys. Chem. B* **2018**, *122*, 7027–7037; j) A. Carlos Borin, S. Mai, P. Marquetand, L. González, *Phys. Chem. Chem. Phys.* **2017**, *19*, 5888–5894; k) R. Xu, Z. Hu, X. Wang, Y. Liu, Z. Zhou, J. Xu, Z. Sun, H. Sun, J. Chen, *J. Phys. Chem. B* **2020**, *124*, 2560–2567.
[6] X. Wang, Y. Yu, Z. Zhou, Y. Liu, Y. Yang, J. Xu, J. Chen, *J. Phys. Chem. B* **2019**, *123*, 5782–5790.
[7] A. Francés-Monerris, M. Lineros-Rosa, M. A. Miranda, V. Lhiaubet-Vallet, A. Monari, *Chem. Commun.* **2020**, *56*, 4404–4407.
[8] M. Lineros-Rosa, A. Francés-Monerris, A. Monari, M. A. Miranda, V. Lhiaubet-Vallet, *Phys. Chem. Chem. Phys.* **2020**, *22*, 25661–25668.
[9] P. M. Hare, C. E. Crespo-Hernández, B. Kohler, *Proc. Natl. Acad. Sci. USA* **2007**, *104*, 435–440.
[10] a) B. M. Pilles, B. Maerz, J. Chen, D. B. Bucher, P. Gilch, B. Kohler, W. Zinth, B. P. Fingerhut, W. J. Schreier, *J. Phys. Chem. A* **2018**, *122*, 4819–4828; b) M. M. Brister, C. E. Crespo-Hernández, *J. Phys. Chem. Lett.* **2019**, *10*, 2156–2161; c) L. Fu, Z. Wang, Y. Liu, X. Wang, R. Xu, W. Liu, J. Chen, J. Xu, *J. Photochem. Photobiol. A* **2020**, *396*, 112491; d) K. Zhang, F. Wang, Y. Jiang, X. Wang, H. Pan, Z. Sun, H. Sun, J. Xu, J. Chen, *J. Phys. Chem. B* **2021**, *125*, 2042–2049.
[11] V. Vendrell-Criado, G. M. Rodríguez-Muñiz, M. C. Cuquerella, V. Lhiaubet-Vallet, M. A. Miranda, *Angew. Chem. Int. Ed.* **2013**, *52*, 6476; *Angew. Chem.* **2013**, *125*, 6604–6607.
[12] A. J. Pepino, J. Segarra-Martí, A. Nenov, R. Improta, M. Garavelli, *J. Phys. Chem. Lett.* **2017**, *8*, 1777–1783.
[13] a) A. W. Parker, C. Y. Lin, M. W. George, M. Towrie, M. K. Kuimova, *J. Phys. Chem. B* **2010**, *114*, 3660–3667; b) Y. Zhang, K. de La Harpe, A. A. Beckstead, L. Martínez-Fernández, R. Improta, B. Kohler, *J. Phys. Chem. Lett.* **2016**, *7*, 950–954; c) M. Kuimova, J. Dyer, M. George, D. Grills, J. Kelly, P. Matousek, A. Parker, X. Sun, M. Towrie, A. Whelan, *Chem. Commun.* **2005**, 1182–1184.
[14] C. E. Crespo-Hernández, D. L. H. Kimberly, K. Bern, *J. Am. Chem. Soc.* **2008**, *130*, 10844.
[15] a) S. Quinn, G. W. Doorley, G. W. Watson, A. J. Cowan, M. W. George, A. W. Parker, K. L. Ronayne, M. Towrie, J. M. Kelly, *Chem. Commun.* **2007**, 2130–2132; b) P. M. Keane, M. Wojdyla, G. W. Doorley, G. W. Watson, I. P. Clark, G. M. Greetham, A. W. Parker, M. Towrie, J. M. Kelly, S. J. Quinn, *J. Am. Chem. Soc.* **2011**, *133*, 4212–4215.
[16] F. J. A. Ferrer, R. Improta, F. Santoro, V. Barone, *Phys. Chem. Chem. Phys.* **2011**, *13*, 17007–17012.
[17] a) M. Berger, I. L. Goldblatt, C. Steel, *J. Am. Chem. Soc.* **1973**, *95*, 1717–1725; b) N. Ohmori, T. Suzuki, M. Ito, *J. Phys. Chem.* **1988**, *92*, 1086–1093; c) S. R. Feenstra, S. J. Park, S. T. Shoujun, *Science* **2005**, *307*, 558–563; d) W.-H. Fang, *Acc. Chem. Res.* **2008**, *41*, 452–457; e) Q. Ou, J. E. Subotnik, *J. Phys. Chem. C* **2013**, *117*, 19839–19849.
[18] M. El-Sayed, *J. Chem. Phys.* **1974**, *60*, 4502–4507.
[19] Z. E. Dance, S. M. Mickley, T. M. Wilson, A. B. Ricks, A. M. Scott, M. A. Ratner, M. R. Wasielewski, *J. Phys. Chem. A* **2008**, *112*, 4194–4201.
[20] a) M. A. Filatov, S. Karuthedath, P. M. Polestshuk, H. Savoie, K. J. Flanagan, C. Sy, E. Sitte, M. Telitchko, F. Laquai, R. W. Boyle, M. O. Senge, *J. Am. Chem. Soc.* **2017**, *139*, 6282–6285; b) Z. Wang, J. Zhao, *Org. Lett.* **2017**, *19*, 4492–4495; c) M. A. Filatov, S. Karuthedath, P. M. Polestshuk, S. Callaghan, K. J. Flanagan, M. Telitchko, T. Wiesner, F. Laquai, M. O. Senge, *Phys. Chem. Chem. Phys.* **2018**, *20*, 8016–8031; d) Y. Hou, T. Biskup, S. Rein, Z. Wang, L. Bussotti, N. Russo, P. Foggi, J. Zhao, M. Di Donato, G. Mazzone, S. Weber, *J. Phys. Chem. C* **2018**, *122*, 27850–27865; e) S. M. Sartor, B. G. McCarthy, R. M. Pearson, G. M. Miyake, N. H. Damrauer, *J. Am. Chem. Soc.* **2018**, *140*, 4778–4781; f) Y. E. Kandrashkin, Z. Wang, A. A. Sukhanov, Y. Hou, X. Zhang, Y. Liu, V. K. Voronkova, J. Zhao, *J. Phys. Chem. Lett.* **2019**, 4157–4163; g) J. T. Buck, A. M. Boudreau, A. DeCarmine, R. W. Wilson, J. Hampsey, T. Mani, *Chem* **2019**, *5*, 138–155; h) M. Lv, Y. Yu, M. E. Sandoval-Salinas, J. Xu, Z. Lei, D. Casanova, Y. Yang, J. Chen, *Angew. Chem. Int. Ed.* **2020**, *59*, 23521; *Angew. Chem.* **2020**, *132*, 23727–22368.
[21] a) S. Mai, M. Pollum, L. Martínez-Fernández, N. Dunn, P. Marquetand, I. Corral, C. E. Crespo-Hernández, L. González, *Nat. Commun.* **2016**, *7*, 13077; b) M. Pollum, L. Martínez-Fernández, C. E. Crespo-Hernández, *Photochemistry of Nucleic Acid Bases and Their Thio- and Aza-Analogues in Solution*, Eds.: M. Barbatti, A. C. Borin, S. Ullrich, Springer International Publishing, Cham, **2015**, pp. 245–327.
[22] S. Arslancan, M.-F. Lara, C. Inés, *Molecules* **2017**, *22*, 998.
[23] a) R. Improta, V. Barone, *Excited States Behavior of Nucleobases in Solution: Insights from Computational Studies*, Eds.: M. Barbatti, A. C. Borin, S. Ullrich, Springer International Publishing, Cham, **2015**, pp. 329–357; b) F. Santoro, V. Barone, T. Gustavsson, R. Improta, *J. Am. Chem. Soc.* **2006**, *128*, 16312–16322; c) T. Gustavsson, N. Sarkar, E. Lazzarotto, D. Markovitsi, V. Barone, R. Improta, *J. Phys. Chem. B* **2006**, *110*, 12843–12847.
[24] Y. Zhang, J. Chen, B. Kohler, *J. Phys. Chem. A* **2013**, *117*, 6771–6780.
[25] J. Snellenburg, S. Laptenok, R. Seger, K. Mullen, I. V. Stokkum, *J. Stata. Softw.* **2012**, *49*, 1–22.
[26] T. Yanai, D. P. Tew, N. C. Handy, *Chem. Phys. Lett.* **2004**, *393*, 51–57.
[27] a) Y. Zhao, N. E. Schultz, D. G. Truhlar, *J. Chem. Theory Comput.* **2006**, *2*, 364; b) Y. Zhao, D. G. Truhlar, *Acc. Chem. Res.* **2008**, *41*, 157–167.

[28] a) J. Tomasi, B. Mennucci, R. Cammi, *Chem. Rev.* **2005**, *105*, 2999–3093; b) S. Miertu, E. Scrocco, J. Tomasi, *Chem. Phys.* **1981**, *55*, 117–129.
[29] R. Improta, F. Santoro, L. Blancafort, *Chem. Rev.* **2016**, *116*, 3540–3593.
[30] J. Segarra-Martí, T. Tran, M. J. Bearpark, *ChemPhotoChem* **2019**, *3*, 856–865.
[31] X. Gao, S. Bai, D. Fazzi, T. Niehaus, M. Barbatti, W. Thiel, *J. Chem. Theory Comput.* **2017**, *13*, 515–524.
[32] Y. Zhang, K. de La Harpe, A. A. Beckstead, R. Improta, B. Kohler, *J. Am. Chem. Soc.* **2015**, *137*, 7059–7062.

Manuscript received: March 3, 2021
Accepted manuscript online: April 15, 2021
Version of record online: May 27, 2021